



Research Article

## Parametric study of natural convection showing effects of geometry, number and orientation of fins on a finned tube system: A numerical approach

Gaurav KRISHNAYATRA<sup>1,\*</sup>, Sulekh TOKAS<sup>1</sup>, Rajesh KUMAR<sup>1</sup>, Mohammad ZUNAID<sup>1</sup>

<sup>1</sup>Department of Mechanical Engineering, Delhi Technological University, Delhi, India

### ARTICLE INFO

#### Article history

Received: 14 March 2020

Accepted: 14 May 2020

#### Keywords:

Natural Convection, Fin Effectiveness, Fin Geometry, Heat Transfer Enhancement

### ABSTRACT

The present study provides a thorough numerical analysis of natural convection heat transfer from a horizontal cylinder with external longitudinal fins. The Three-dimensional(3D) forms of Continuity, Navier-stokes, and the energy equations have been solved to understand the flow field and temperature distribution using the Ansys Fluent software. The purpose of the study is to investigate the effects of fin length  $L_f$ , fin thickness ( $t$ ), number of fins ( $N$ ) and material of fin (Aluminum & Steel) on the parameters namely, the heat transfer rate from the inner isothermal wall and effectiveness ( $Q^*$ ) of the system for a constant Rayleigh number in the laminar range ( $Ra \leq 10^6$ ). Additionally, the effect of two different orientations (A&B) of fins has been discussed. Orientation-A consists of fins starting from horizontal plane placed at equal angular spacing subsequently, whereas the fins in orientation-B originate from the vertical plane followed with equal angular spacing. Non-dimensional fin length ( $L^*$ ) is being varied from 0.222 to 2, non-dimensional fin thickness ( $t^*$ ) as 0.022 ~0.044 and the number of fins ( $N$ ) between 6~24. It is observed that for a fixed number of fins there exists an optimum fin length and for a fixed fin length there exists an optimum fin thickness & an optimum number of fins. For a fixed number of fins there exist an optimum fin length and maximum effectiveness, the maximum possible effectiveness for the taken fin-tube system is 4.34 for 12 fins. The maximum effectiveness reported in the current study was 1.86 for  $L^*=0.444$ ,  $t^*=0.022$  and  $N=12$ . Furthermore, the optimum length for  $N=12$  came out to be  $L^*=1.8$ .

**Cite this article as:** Gaurav K, Sulekh T, Rajesh K, Mohammad Z. Parametric study of natural convection showing effects of geometry, number and orientation of fins on a finned tube system: A numerical approach. J Ther Eng 2022;8(2):268–285.

#### \*Corresponding author.

\*E-mail address: [gauravkrishnayatra\\_mt2k18@dtu.ac.in](mailto:gauravkrishnayatra_mt2k18@dtu.ac.in)

This paper was recommended for publication in revised form by Regional Editor  
Younes Menni



## INTRODUCTION

For the enhancement of functionality, efficiency and reliability of advanced components implied in a system for effective heat dissipation, Cooling and maintaining the temperature of the system below a certain range becomes of utmost importance. Various methods have been studied and researched for this purpose including the natural and forced convection heat transfer [1]. Natural convection heat transfer carries a wide range of applications in the domain of microelectronics, electrical devices, power generation sector, automobiles, power transmission lines, Latent heat storage devices involving phase change materials (PCM), etc. [2-6]. Most of the applications have a basic requirement of effective dissipation of generated heat in order to maintain the temperature of operating devices within the safe operational limit. There is no requirement of external power in the case of natural convection since it involves buoyancy-driven flow making it an economically feasible method. The geometry under investigation can be characterized as a heat exchanger of the fin-tube type. These heat exchangers carry relevance in chemicals, petrochemicals industries, oil & gas sector, cryogenics, refrigeration [7]. The longitudinal fin tube type arrangement is widely used in shell and tube type heat exchangers namely in double-pipe and multi-pipe heat exchangers where the longitudinal finned tube is fit inside a larger tube shell.

Study of natural convection over different bodies placed in ambient air is a well-researched field and has been explored extensively with the help of experimental study and numerical solutions using various techniques. The research work of Churchill & Chu [8] gave a benchmark relation for the solid cylinder under natural convection covering a wide range of Rayleigh number which is still being used by various researchers. Morgan [9] conducted various experiments for isothermal solid cylinder under natural convection and a correlation was provided for a horizontal solid cylinder under isothermal boundary condition. Finite Difference Method (FDM) discretization was broadly used to numerically solve the governing equations, however, as the technology advanced the drawbacks begin to come in the picture. Kwon and Kuehn [10] numerically solved conjugate heat transfer laminar natural convection from a solid isothermal cylinder with one infinitely long vertical plate-fin and developed various correlations to pre-visualize both local and total heat transfer rates from the cylinder. Tolpadi and Kuehn [11] used finite-difference technique to perform three-dimensional parametric study for a transversely finned horizontal cylinder under natural convection and concluded that for a particular material and thickness of fin, an optimum number of fins exist where the total heat transfer maximizes.

Depending on the application, fins can be added on a flat surface or a cylindrical surface to escalate the heat transfer from the base wall, as it increases the total heat transfer area. Numerous studies have been performed on the horizontal

finned solid cylinder with both radial and longitudinal fins. Yuncu & Anbar [12] experimentally examined the free convection heat transfer from 15 different array of rectangular fin in the atmosphere. The purpose behind the study was to explore the effects of fins height, fin spacing and the temperature difference between the fluid & base temperature and they found that the heat transfer rate firmly depends on the number of fins and the fin height to fin spacing ratio. Abu-hijleh [13] studied the natural convection heat transfer around the horizontal solid cylinder with high conductivity fins using the finite-difference numerical technique for a wide range of Rayleigh numbers and concluded that there exists an optimum fin number and fin height for which the Nusselt number is maximum. Abu-hijleh [14] illustrates the optimization of longitudinal fins for maximum heat transfer and the cost factor was also incorporated in the analysis of optimization. Wu & Tao [15] computed natural convection heat transfer from a compound horizontal tube with external longitudinal fins where the heat transfer was taking place from ambient air to the inside of the compound tube with isothermal inner wall boundary condition. Senapati et al. [16] investigated natural convection heat transfer over annular finned horizontal & vertical cylinder and a suitable correlation for Nusselt number was also provided using the regression analysis. Acharya et al. [17] conducted numerical experiments on heat transfer from unfinned hollow horizontal cylinder and calculated heat flux on both the inner and outer wall of the hollow cylinder with air inside the cylinder participating in the heat transfer, a correlation for Nusselt number with the independent variable being the geometrical parameters and Rayleigh number was developed using the regression analysis. Foroushani et al. [18] utilized the extended newton formulation to address the three-temperature heat transfer problem of natural convection for isothermal walls. Additionally, simple correlations were developed for individual heat transfer rates. Yildiz [19] studied the natural convection heat transfer phenomenon on a vertical and inclined plate with the angle of inclination between 20°~45° from the vertical plane. Rath & Dash [20] numerically studied natural convection application in the case of a 3-dimensional stack of thin hollow horizontal cylinders and gave empirical correlations for the Nusselt number.

A further work of natural convection with nanofluids & porous mediums have attracted several researchers since it is an effective way to enhance the heat transfer rate and can be widely used in various applications [21]. Gorla & Chamkha [22] closely studied the natural convection over a non-isothermal vertical plate in porous medium with saturated nanofluid. While Mahfoud & Bendjaghloli [23] examined it in the case of conical container filled with nanofluid. Zaraki et al. [24] performed a theoretical analysis of natural convection heat & mass transfer over a flat plate to understand the role of size, shape, and type of nanoparticles used in the base fluid. The recent work of Dogonchi et al. [25]

presented an analysis of nanofluid natural convection for a square enclosure with a circular wavy heater subjected to the magnetic field with the help of control volume finite element method.

Though a wide range of literature is available on the natural convection heat transfer, however fewer investigations have been performed on the hollow horizontal tube with external axial longitudinal fins attached to it while considering the effect of conduction resistance due to the tube thickness as visible in the thermal circuit in figure 1 and different orientation of the fins (A & B) as shown in 3 a) and b) respectively.

In a heated hollow tube with the isothermal inner wall, the heat transfer takes place from the inner surface and hence the conduction resistance offered by the thickness of the tube comes into the picture whereas in solid cylinder only the outer surface takes part in the heat transfer as illustrated in the thermal resistance circuit in Figure 1. Therefore, the current study provides a thorough numerical investigation of conjugate heat transfer from a horizontal tube with external fins along with capturing the flow physics with pictorial representation of velocity vectors and thermal plumes. Moreover, the effect of parameters including the thickness of fin ( $t$ ), length of fins ( $L_f$ ), number of fins ( $N$ ) and material of fins on performance indicators namely the heat flux ( $q$ ) and effectiveness ( $Q^*$ ) are presented in various graphs. All the geometrical variables are presented in the dimensionless form like non-dimensional heat flux

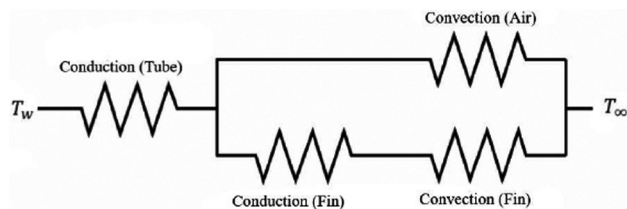


Figure 1. Thermal Resistance Circuit for the fin-tube system.

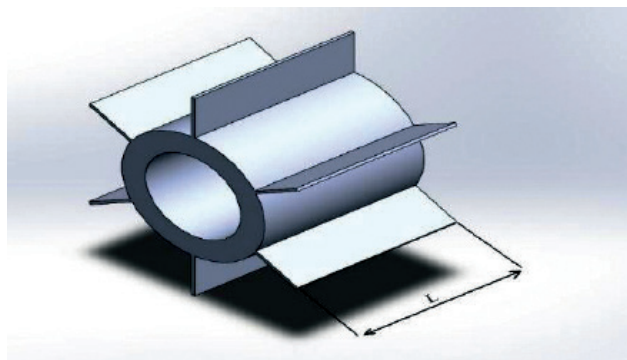


Figure 2. Three-Dimensional representation of the model.

(NDHF) which represents the ratio heat transfer rate per unit area for the fin-tube system and the tube without fins, non-dimensional fin length ( $L^*$ ) and non-dimensional fin thickness ( $t^*$ ). Simulations are performed on the commercial software Ansys Fluent, numerical computation is used over experimentation for different geometrical model because using computational fluid dynamics is cost-effective and time saving.

## GOVERNING EQUATIONS AND MATHEMATICAL MODELLING

### Physical Description

The basic geometry of the chosen fin-tube type heat exchanger is depicted in Figure 2. It consists of a tube horizontally oriented and rectangular longitudinal fins of equal length put out at an equal angular spacing on the outer periphery of the tube to enhance the net rate of heat transfer from the inner isothermal wall of the tube.

The study was performed choosing two different materials namely Aluminium ( $K_{al} = 202.43$  W/mK) and Stainless Steel ( $K_{st} = 16.2$  W/mK) to understand the effect of various fin parameters with different materials of construction on the performance of the system.

Figure 3(a) and Figure 3(b) shows schematic diagram of lateral cross-sectional of the geometry with six fins. Although the number of fins in this case is the same on the outer surface of the tube, the orientation of fins is different which greatly influence the flow pattern in the buoyancy driven flow and hence impact the total heat transfer rate. Orientation-A consists of fins at the angles of  $30^\circ$ ,  $90^\circ$  and  $150^\circ$  from the vertical axis whereas in Orientation-B fins can be visualised at an angle of  $0^\circ$ ,  $60^\circ$  and  $120^\circ$  from the vertical plane. Present study provides a close comparison

Table 1. Materials & their thermal conductivities

Material	Thermal Conductivity (W/mK)
Aluminium	202.43
Stainless Steel	16.2

Table 2. Geometrical dimensions of the 3D model

Parameter	Value
Inner diameter of cylinder ( $D_i$ )	20 mm
Outer diameter of cylinder ( $D_o$ )	25 mm
Domain Diameter ( $D_d$ )	150 mm
Fin length ( $t^*$ )	0.0222 – 2.0
Fin Thickness ( $L^*$ )	0.0222 – 2

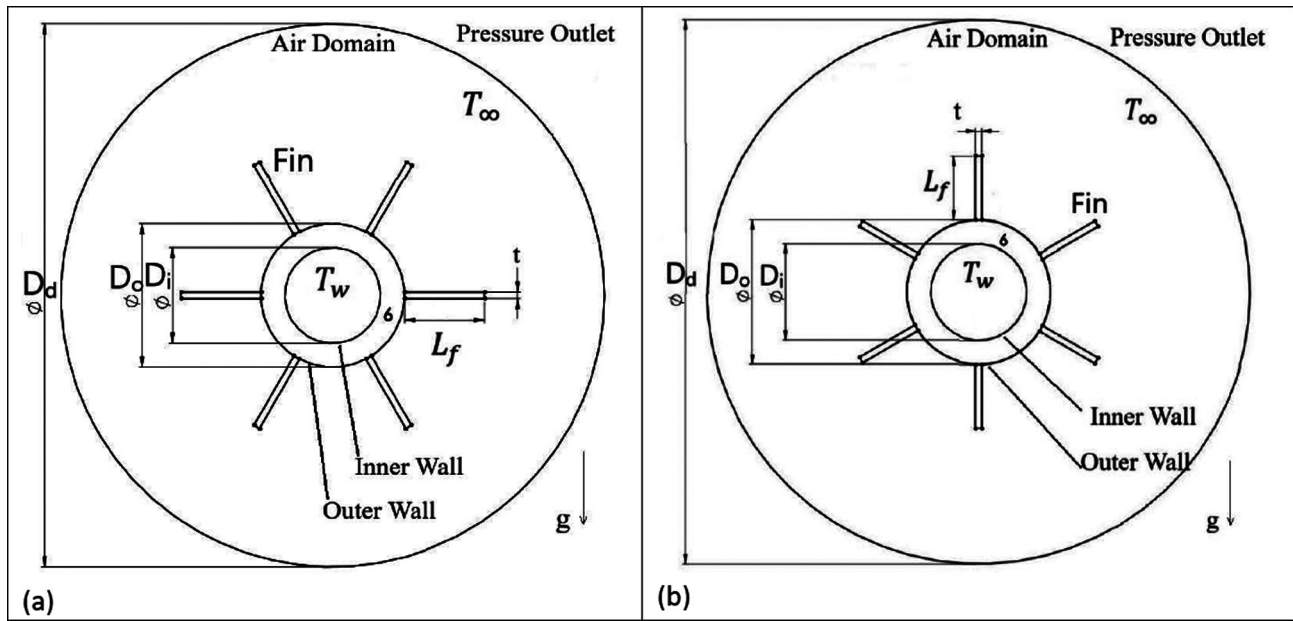


Figure 3. a) Schematic representation of Orientation A, b) Schematic representation of Orientation B.

between these two different types of orientation with the help of visualization of temperature plumes and velocity vector contours.

**Governing Equations and Boundary Conditions**

The governing equations using the bousinessq approximation can be written as follows in the tensorial form [36]. The following assumptions have been made for conducting the following study:

1. The air flow is steady, laminar and incompressible.
2. The bousinessq approximation is assumed at the .
3. The inner wall temperature is 290 K and the ambient temperature is 310 K.

Continuity equation:

$$\frac{\partial}{\partial x_i}(U_i) = 0 \tag{1}$$

Momentum equation:

$$\frac{D}{Dt}(\rho U_i) = -\frac{\partial p}{\partial x_i} + \frac{\partial}{\partial x_j} \left[ \mu \left( \frac{\partial U_i}{\partial x_j} + \frac{\partial U_j}{\partial x_i} \right) \right] + (\rho - \rho_\infty) g_i \tag{2}$$

Energy equation:

$$\frac{D}{Dt}(\rho c_p T) = \frac{\partial}{\partial x_i} \left( k \frac{\partial T}{\partial x_i} \right) \tag{3}$$

Energy equation for solid conduction in fin:

$$\frac{\partial}{\partial x_i} \left( \frac{\partial T}{\partial x_i} \right) = 0 \tag{4}$$

The density of air is calculated by the equation of state as

$$\rho = \frac{p}{RT} \tag{5}$$

Where p is the pressure which is constant at atmospheric pressure and R is the gas constant. The various boundary conditions to solve the governing equations mentioned above are as follows:

The inner surface of the hollow tube is isothermal

$$T = T_w \tag{6}$$

No slip condition on all the walls is given as

$$u = v = w = 0 \tag{7}$$

At the air-fin interface, the coupled boundary condition is used in order to maintain the continuity of heat and temperature

$$k_{so} \left( \frac{\partial T_{so}}{\partial n} \right)_{interface} = k_{fl} \left( \frac{\partial T_{fl}}{\partial n} \right)_{interface} \tag{8}$$

$$T_{so} = T_{fl} \tag{9}$$

Since the flow is buoyancy driven, air enters and leaves from the outer surface of the cylindrical domain of air considered, thus it is subjected to pressure outlet boundary condition.

$$T = T_{\infty} \ \& \ p = p_{atm} \tag{10}$$

The thermo-physical properties of air taken for this study is at the mean bulk temperature  $(T_w + T_{\infty})/2 = T_b = 300 \text{ K}$ .

**Other Parameters**

The Newton’s law of convection is given by

$$Q = hA_t (T_w - T_{\infty}) \tag{11}$$

Where h is the overall average heat transfer coefficient based on both the unfinned and finned surface area.  $A_t$  is the total heat transfer area given as

$$A_t = NA_{fin} + A_{unfin} \tag{12}$$

Where N is the number of fins on the outer periphery of the tube. The heat transfer coefficient can be calculated from Equation (10) and Nusselt number, which can be explained as the enhancement of heat transfer coefficient when a fluid is flowing with respect to still fluid. based on the outer diameter of the tube can be written as

$$Nu = \frac{hD_0}{k_{fl}} \tag{13}$$

Similarly, Rayleigh number, it is the ratio of buoyancy forces and the viscous forces which governs the natural convection phenomena, based on the outer diameter of the tube can be computed as:

$$Ra_D = \frac{g\beta\Delta TD^3}{\alpha\nu} \tag{14}$$

**Table 3.** Thermophysical properties of air at  $T_b = 300 \text{ K}$

Property	Value
Specific Heat ( $J/kg.K$ )	1006
Kinematic Viscosity ( $m^2/s$ )	$1.552 \times 10^{-5}$
Density ( $kg/m^3$ )	1.184
Thermal Conductivity ( $W/m.K$ )	0.02624
Coefficient of Thermal Expansion ( $1/K$ )	0.00338

**GRID INDEPENDENCE TEST**

The geometrical models prepared in Solidworks CAD software were imported to Fluent, where they were discretized using Ansys Mesh which uses the Finite Volume Method. Then the governing equations are converted to

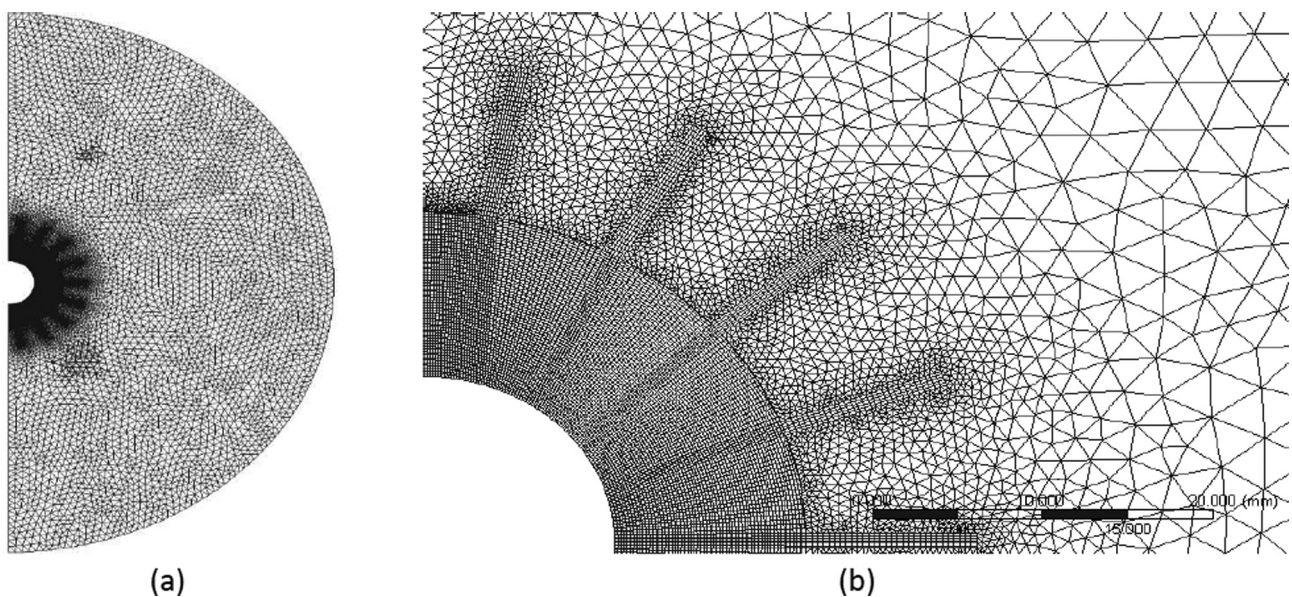


**Figure 4.** a) Cross-sectional view of the meshing of full model; b) Cross-sectional view of the meshing of zoomed in area.

algebraic form to get integrated over each discretized element and are solved using numerical techniques. The momentum and energy were spatially discretized for a second-order upwind while for pressure, body weighted law was used. Pressure based solver was selected and the SIMPLE algorithm was used for pressure-velocity coupling. The residual for continuity and momentum was taken at  $10^{-3}$  and for energy residual tolerance was set to  $10^{-6}$ . The system on which the simulations were performed had 16 GB DDR4 ram with 8 core processor (CPU) having maximum clock speed of 2.4 Ghz and 2 GB graphic processor (GPU).

The cross-sectional view of the generated grid is presented in Figure 4(a) in order to save the computational resources, symmetry about the vertical midplane is considered. The solid domain of the tube and fins contain structured hex elements whereas tetra elements are used in the flow domain due to the complexity of this domain. The elements are very fine near the wall to efficiently capture the flow physics and grow coarse away from the body in the fluid domain as seen in Figure 4(b).

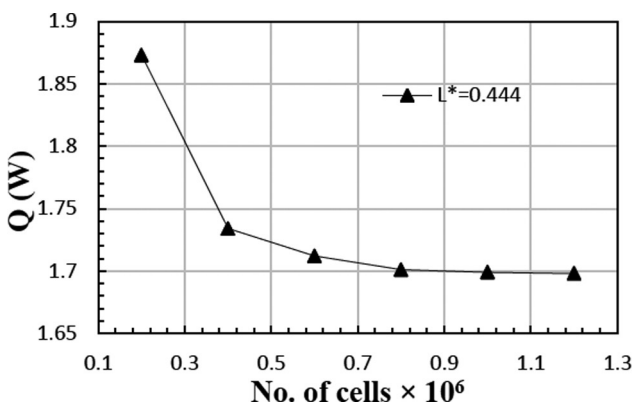
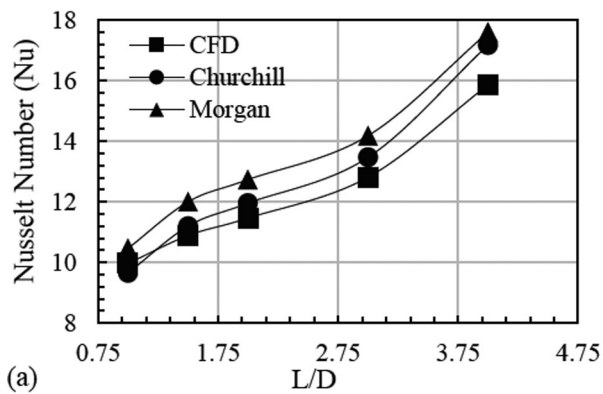


Figure 5. Grid independence test plot.



Grid independence test was performed to make the result of the simulation free from the size of the element resulting in better accuracy of the numerical solution. The simulations for the elements of order  $10^5$  took relatively less time than  $10^6$ , roughly 10 hours for series processing with 1 core and for parallel processing with 4 cores it took about 3 hrs for solution. Figure 5 illustrates the variation of total heat transfer ( $Q$ ) with the number of elements for a specific case of diameter ratio ( $D^*$ ) = 2,  $L^*$  = 0.444 and  $N$  = 30. Initially a steep drop in the heat transfer is visible with an increase in the number of elements however after  $1 \times 10^6$  cells the variation in  $Q$  is much below 1%.

**VALIDATION TEST**

For the purpose of validation of current numerical results, two different validation tests were performed. First test made a comparison of Nusselt number for solid horizontal cylinder under natural convection obtained from CFD with that of the available correlations by [8] and [9] for solid cylinder at different  $L/D$  ratios. Second validation test was performed using the correlation given by [26] for a horizontal tube with external annular fins subjected to natural convection.

The Nusselt number correlation given by [8] which is valid for a range of  $10^{-11} \leq Ra_D \leq 10^9$ ,

$$Nu = \left[ 0.6 + \frac{0.387(Ra_D)^{1/6}}{\left\{ 1 + \left( \frac{0.559}{Pr} \right)^{9/16} \right\}^{8/27}} \right]^2 \tag{15}$$

The correlation given by [9] is valid for  $10^4 \leq Ra_D \leq 10^9$

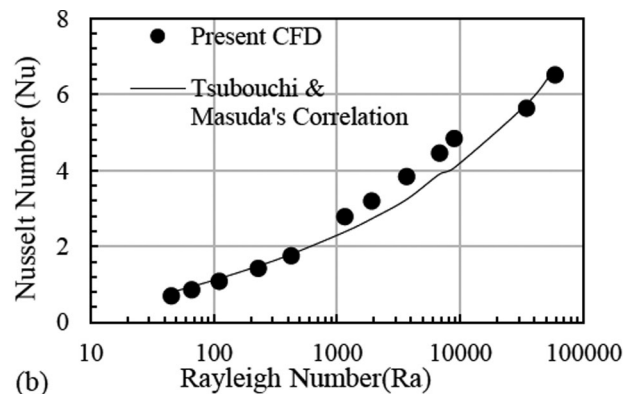


Figure 6. a) Nusselt number as a function of  $L/D$  ratio for current CFD, Churchill & Chu's relation [8] and Morgan's Relation [9]; b) Nusselt number as function of Rayleigh number for current CFD and Tsubouchi & Masuda's relation [26].

$$Nu = 0.48(Ra_D^{0.25}) \quad (16)$$

For [26] correlation showing the Nusselt number where the fin spacing is treated as the characteristic length as a function of Rayleigh number based on the fin spacing as well.

$$Nu_s = \frac{Ra_s}{12\pi} \left\{ 2 - e^{-(C/Ra_s)^{3/4}} - e^{-B(C/Ra_s)^{3/4}} \right\} \quad (17)$$

Where  $Ra_s$  is the Elenbaas Rayleigh number [26]

$$Ra_s = \frac{g\beta(T_w - T_\infty)S^3}{\nu\alpha} \left( \frac{S}{D} \right) \quad (18)$$

And the rest of the components of Equation (17) are explained below

$$B = \left( \frac{0.17}{\xi} \right) + e^{-(4.8/\xi)} \quad (19)$$

$$C = \left\{ \frac{23.7 - 1.1 \left[ 1 + (152/\xi^2) \right]^{1/2}}{1 + B} \right\}^{3/4} \quad (20)$$

$$\xi = \frac{D_o + 2L_f}{D_o} \quad (21)$$

Figure 6(b) presents the variation of Nusselt number with a wide range of Rayleigh number ( $10^2 \leq Ra \leq 10^5$ ) covering the laminar natural convection heat transfer. It is inferred from the validation tests that the results obtained numerically are of good accuracy, hence the numerical method picked for the current study are expected to give

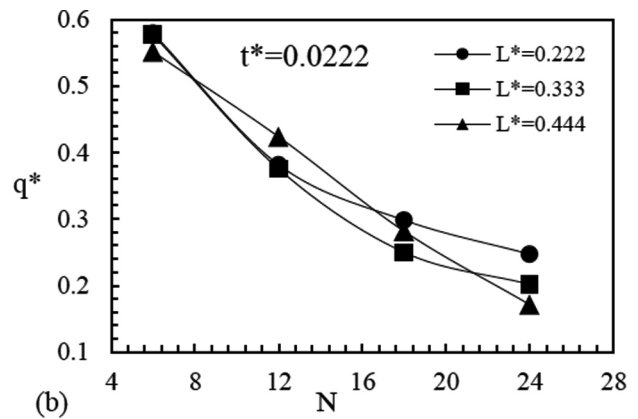
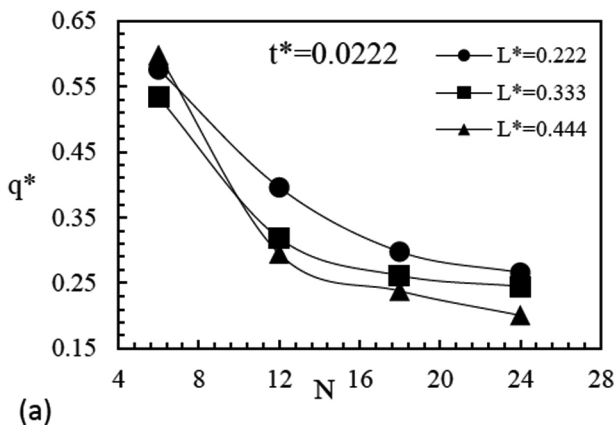


Figure 7. a) Non-Dimensional Heat flux as a function of Number of Fins for Orientation A for  $t^* = 0.0222$ ; b) Non-Dimensional Heat flux as a function of Number of Fins for Orientation B for  $t^* = 0.0222$ .

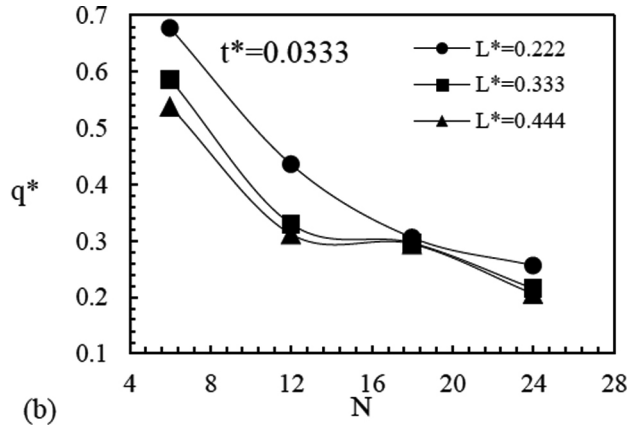
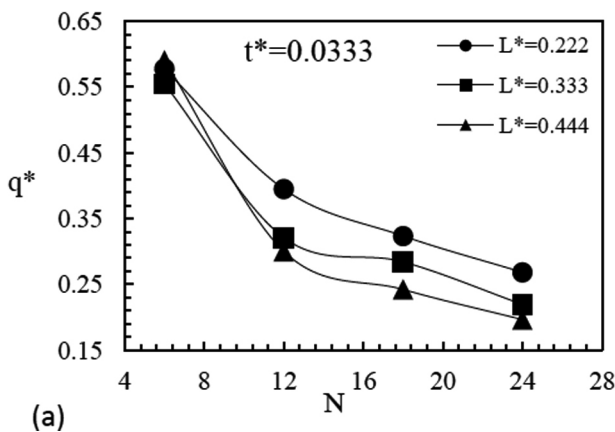
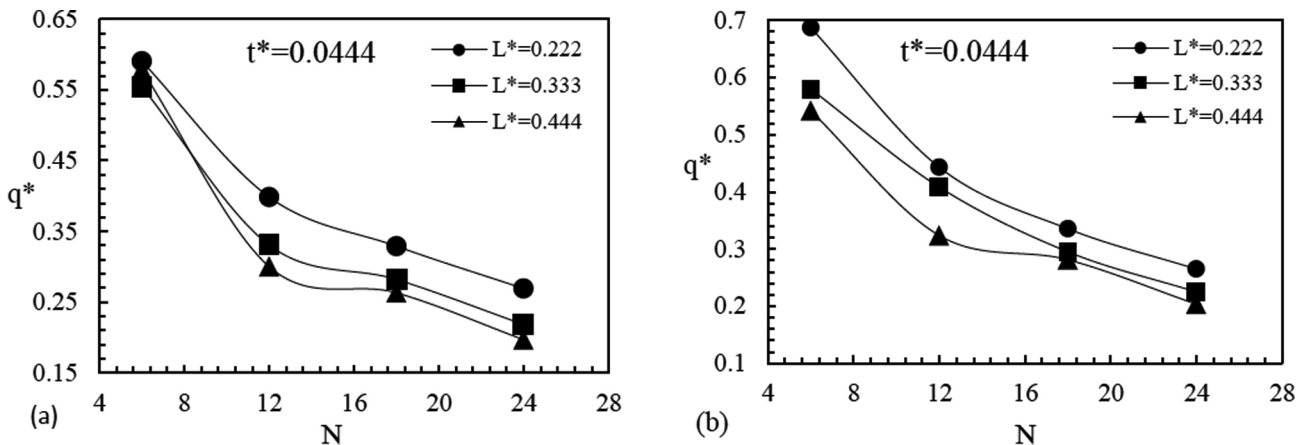


Figure 8. a) Non-Dimensional Heat flux as a function Number of Fins for Orientation A for  $t^* = 0.0333$ ; b) Non-Dimensional Heat flux as a function of Number of Fins for Orientation B for  $t^* = 0.0333$ .



**Figure 9.** a) Non-Dimensional Heat flux as a function of Number of Fins for Orientation A; b) Non-Dimensional Heat flux as a function of Number of Fins for Orientation B.

precise results for the conjugate natural convection heat transfer.

## RESULTS AND DISCUSSION

The Current study involves an intensive comparison of Orientation A and B on the basis of thermal and fluid parameters with respect to change in fin length, fin thickness and the number of fins attached on the outer surface of the hollow cylinder for a constant Rayleigh number. The representation of data is done in the form of fin length to outer diameter ratio ( $L^*$ ) which is ranging from 0.222 to 2 and fin thickness to outer diameter ratio ( $t^*$ ) varying from 0.0222 to 0.0444. The studies on natural convection phenomena conducted by [16] involved a solid cylinder with fins on the outer isothermal surface and [18] had conducted a numerical study on solid and hollow cylinder suspended in the air without fins, in the present study the gap between the two is potentially covered where the horizontal hollow cylinder with isothermal boundary condition on the inner wall having fins attached to the outer surface is subjected to natural convection with variation in fin geometry. It is to achieve a conceivable optimization in effectiveness and heat transfer when there are geometrical constraints for fin geometry. Thermal system such as this one can be used in the cooling of microprocessors, electronics equipment and can also be used as heat exchanger involving phase change at the inner region of the horizontal cylinder. This section involves temperature contours of certain selected geometries that represent the thermal boundary layer under steady-state condition along with the velocity streamlines giving a clear representation of how the air particles behave as they move in the positive Y direction. Velocity vectors

are also being represented in a section that differentiates the behaviour of small vortices formation for the two orientations. It is quite critical to discuss and compare the thermal characteristics such as non-dimensional heat flux and effectiveness. Non-dimensional heat flux (NDHF) ( $q^*$ ) in this particular study is taken as the ratio of heat flux from CFD simulations of the fin-tube system and heat flux from CFD simulations of the unfinned system, this parameter is signifying the heat transfer rate per unit area with respect to cylinder without fins. Effectiveness ( $Q^*$ ) is the ratio of the total rate of heat transfer of fin-tube system and of the tube without fins.

In the following discussion, Figure 7-9 show the non-dimensional heat flux with respect to number of fins for constant fin thickness with the comparison of  $q^*$  for different fin length. The non-dimensional heat flux is the ratio of heat flux for the geometrical model taken and the heat flux for solid cylinder of the same diameter i.e. 45mm, this essentially incorporates the amount of material being used and consequently the cost of fabricating a fin-tube system with a longitudinal fin at the outer surface. Figure 7 is for  $t^* = 0.0222$ , it is observed that in Orientation-A, the NDHF is highest for the  $L^* = 0.444$  for  $N = 6$  however, as the number of fins is increase NDHF for the same fin length becomes lower than  $L^* = 0.333$  & 0.222. For Orientation-B the behavior of NDHF is rather chaotic. Initially  $L^* = 0.444$  has the lowest value among the other  $L^*$ , but with increasing  $N$  value the NDHF for  $L^* = 0.222$  & 0.333 becomes lower for  $N=12$  and then continues to be higher for consequent  $N$  values. The Figure 8 and Figure 9 represent NDHF for  $t^* = 0.0333$ . It is observed that in Orientation-A the behavior of NDHF is same as it was for  $t^* = 0.0444$ , however for Orientation-B the NDHF is decreasing with increasing  $N$ .

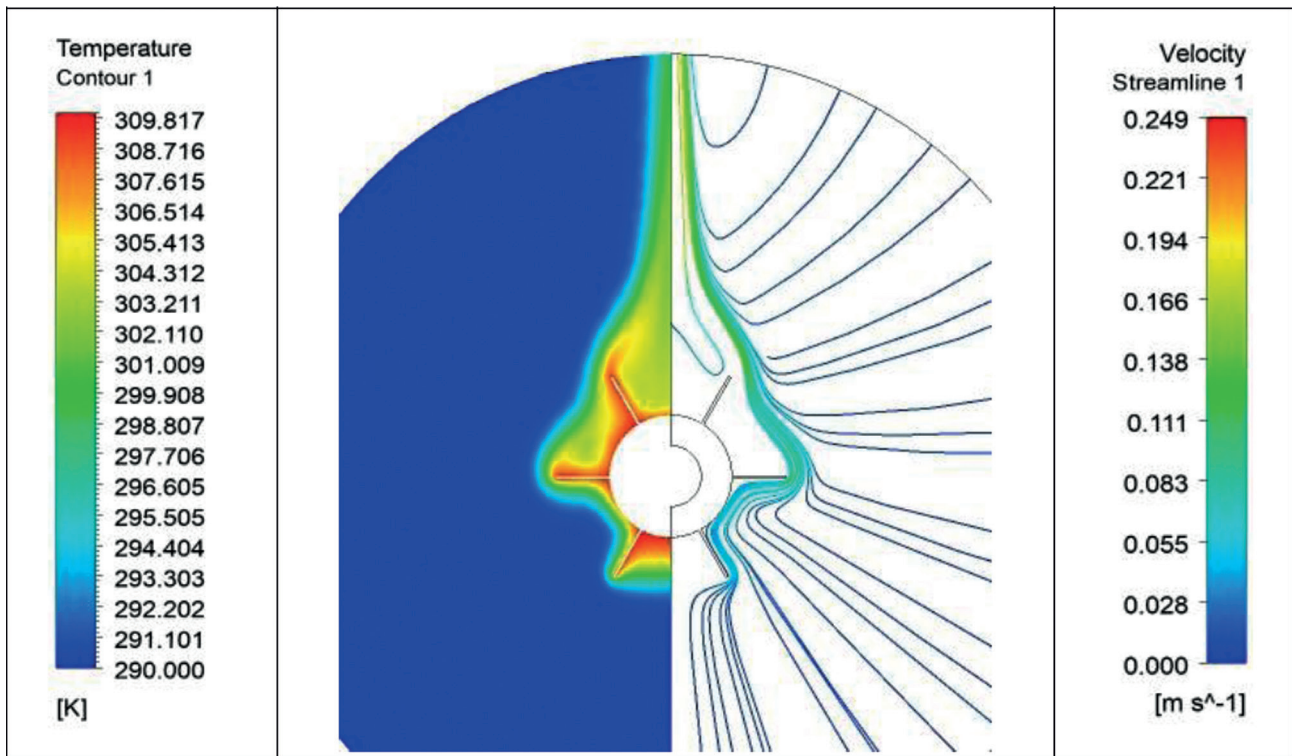


Figure 10. Thermal boundary layer and Velocity Streamlines for  $N = 6$ ,  $t^* = 0.0222$  and  $L^* = 0.444$  Orientation A.

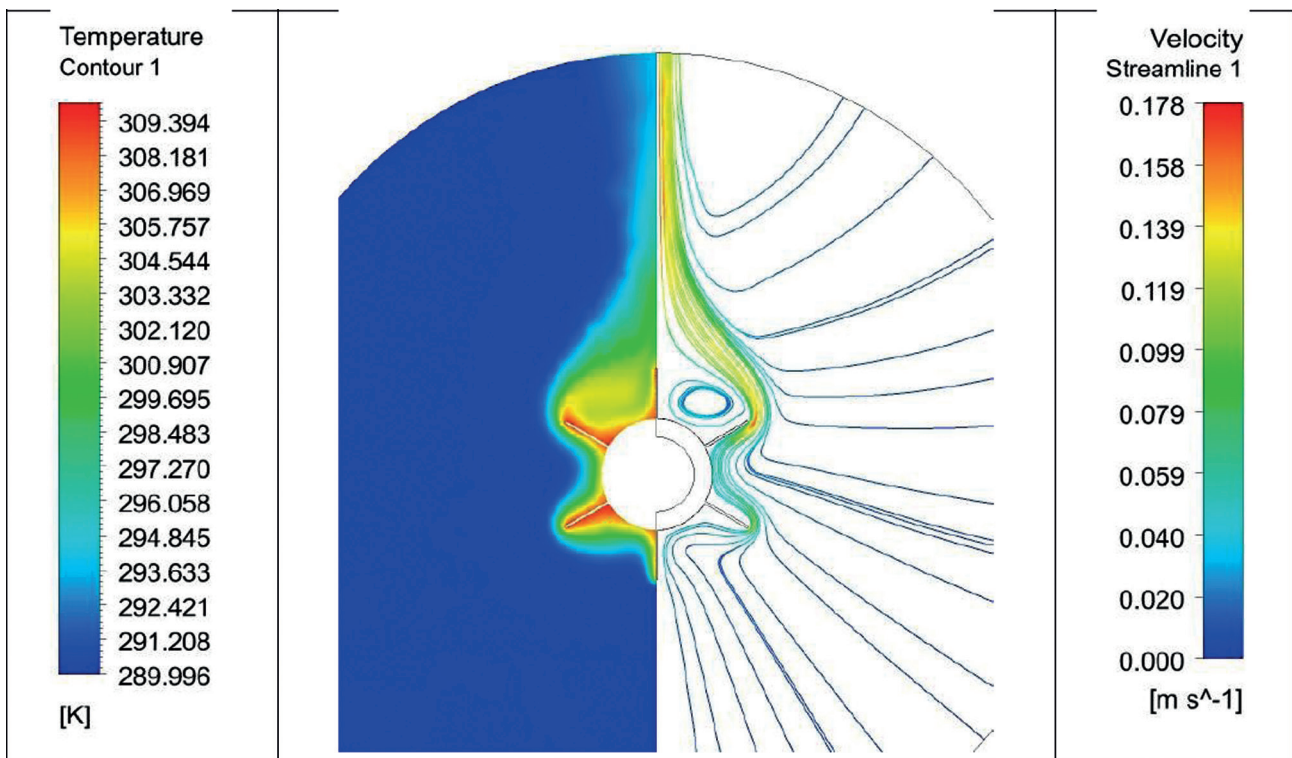


Figure 11. Thermal boundary layer and Velocity Streamlines for  $N=6$ ,  $t^*=0.0222$  and  $L^* = 0.444$ , Orientation B.

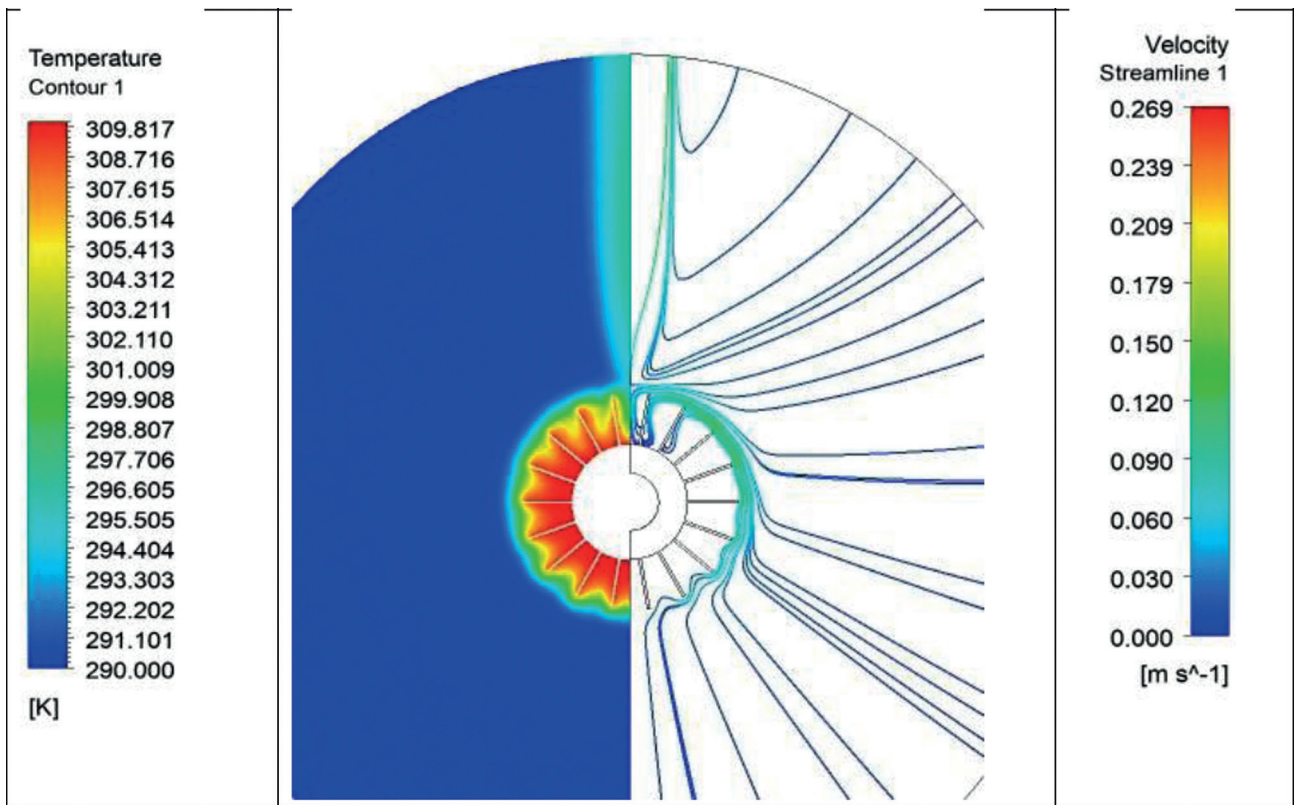


Figure 12. Thermal boundary layer and Velocity Streamlines for  $N = 18$ ,  $t^* = 0.0222$  and  $L^* = 0.444$ , Orientation A.

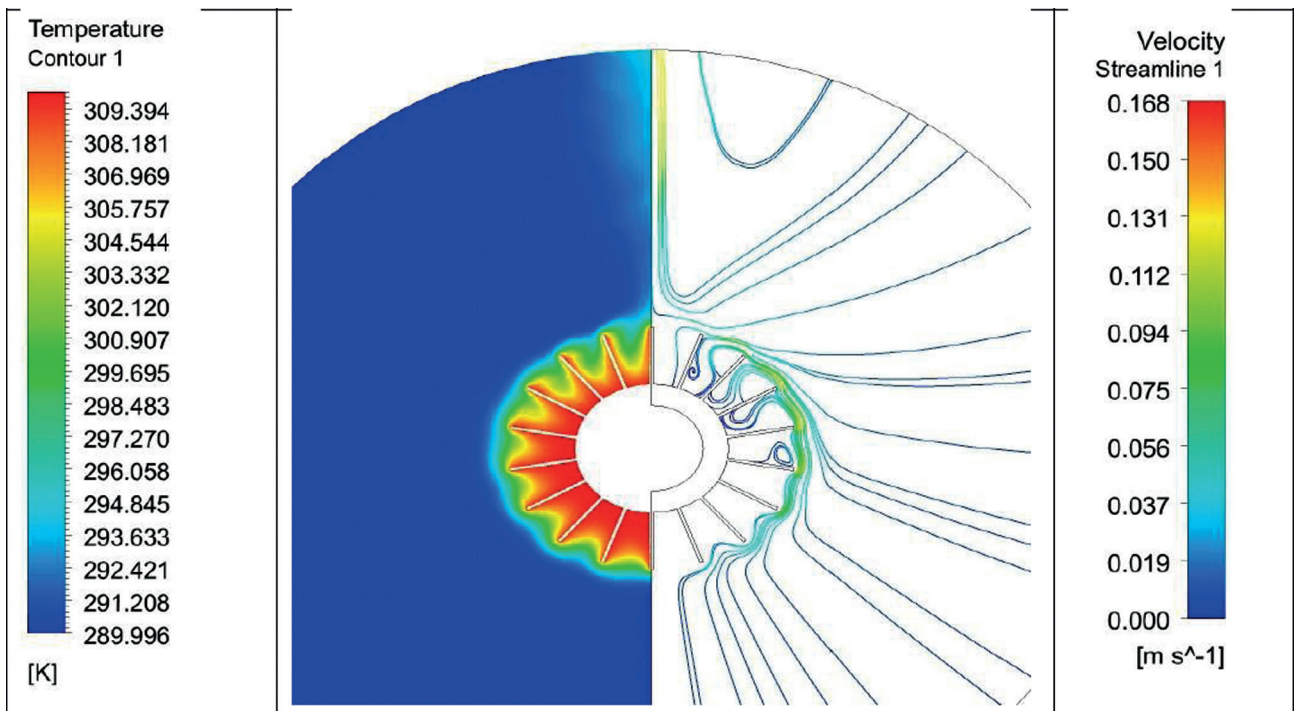
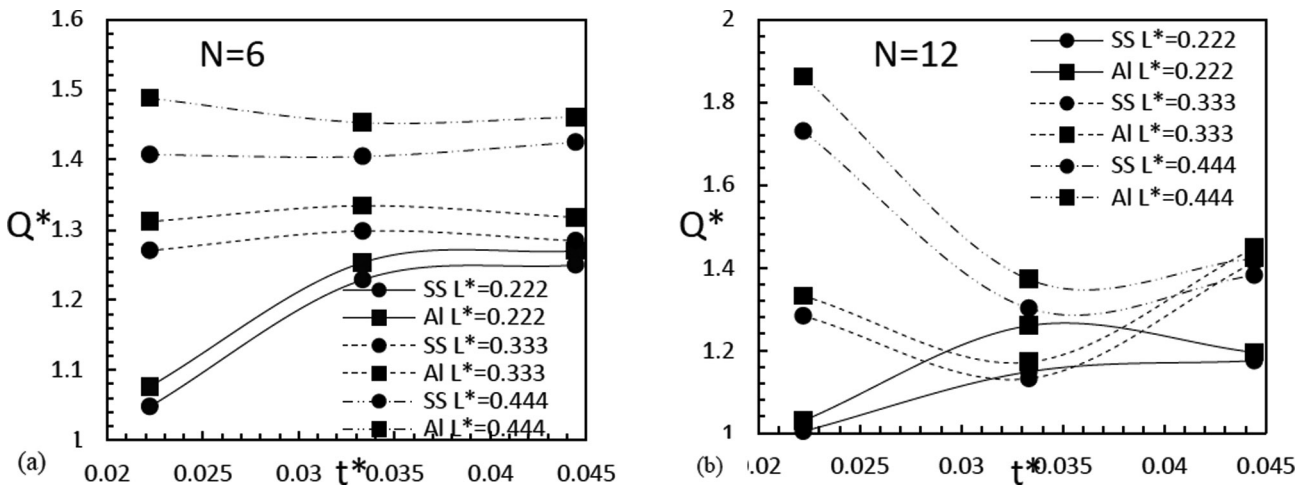


Figure 13. Thermal boundary layer and Velocity Streamlines for  $N = 18$ ,  $t^* = 0.0222$  and  $L^* = 0.444$ , Orientation B.



**Figure 14.** a) Effectiveness shown in relation of non-dimensional fin thickness for Aluminium versus Steel  $N = 6$ ; b) Effectiveness shown in relation of non-dimensional fin thickness for Aluminium versus Steel  $N = 12$ .

**Table 4.** Optimum number of fins and optimum effectiveness for  $L^*$  and  $t^*$

$L^*$	$t^*$	$N_{opt}$		$Q^*_{opt}$	
		A	B	A	B
0.222	0.0222	24	24	1.17	1.08
	0.0333	24	12	1.18	1.26
	0.0444	24	6	1.18	1.27
0.333	0.0222	24	12	1.49	1.33
	0.0333	18	18	1.37	1.42
	0.0444	18	12	1.35	1.44
0.444	0.0222	6	12	1.61	1.86
	0.0333	24	18	1.59	1.79
	0.0444	18	18	1.60	1.71

Figure 10, Figure 11, Figure 12, and Figure 13 are showing the temperature contours and the velocity streamlines for  $N = 6$  and 18 for both the orientations. From Figure 10 and Figure 11 depicts the thermal boundary layer and velocity streamlines for  $t^* = 0.0222$  and  $L^* = 0.444$ , the thermal boundary layer merely represents the ability of heat to penetrate layers of fluid as it moves away from the heated surface with respect to fluid in motion. From the figures, it is convincingly clear that orientation-A has a thicker thermal boundary layer relative to orientation-B, this might decrease the rate of heat transfer for orientation-A but the velocity streamline contours show that the velocity of air is increasing at a greater rate than it is for orientation-B. Figure 12 and Figure 13 are showing the thermal boundary layer and velocity streamlines for  $N=18$ ,  $t^* = 0.0222$  and  $L^* = 0.444$ . It is observed that the temperature gradient is

lower and the velocity of the air particles is lower than that for  $N=6$ , as the number of fins increase the resistance to flow is also increasing which as a result decreases the rate of heat transfer, however, it is compensated by the much more increase in the overall surface area hence the total heat transfer increases.

Figure 14 gives the comparison of the two materials taken up for investigation were Aluminium ( $K_{al} = 202.43$  W/mK) and Stainless Steel ( $K_{st} = 16.2$  W/mK). By understanding the thermal resistance chart given in Figure 1, the conductive thermal resistance offered is quite low in comparison to convective thermal resistance perceived at the outer surface of the fin-tube system. Even though the impact of conductivity is low, the choosing of system's material is important with respect to the costing involved. From the plots given in Figure 14, a comparison of Al and

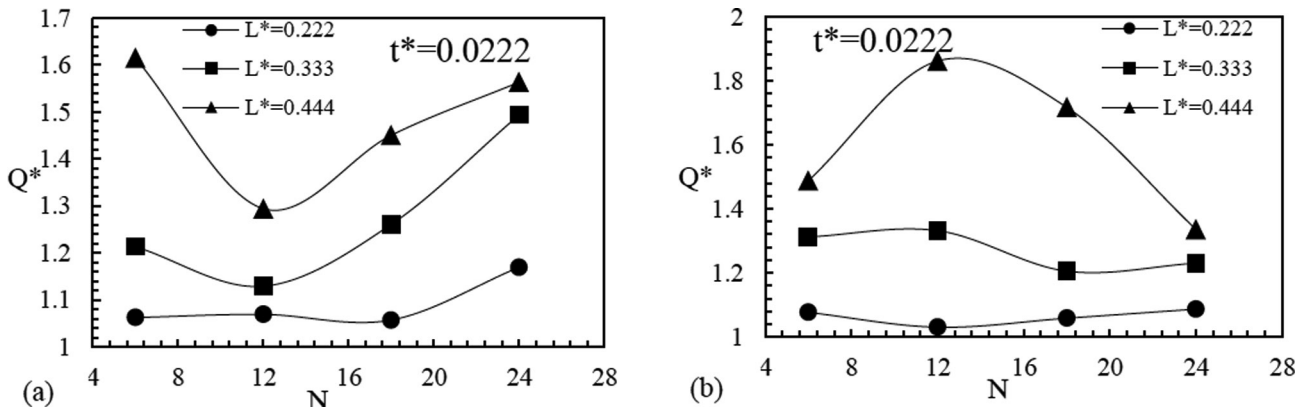


Figure 15. a) Effectiveness as a relation of Number of Fins for  $t^* = 0.0222$ , Orientation A; b) Effectiveness as a relation of Number of Fins for  $t^* = 0.0222$ , Orientation B.

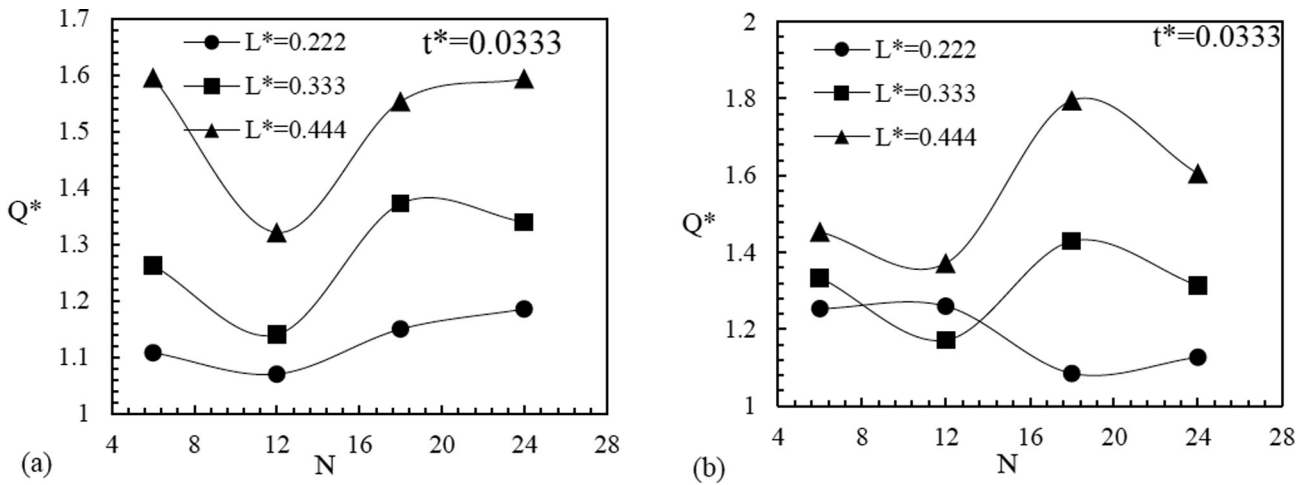


Figure 16. a) Effectiveness as a relation of Number of Fins for  $t^* = 0.0333$  Orientation A; b) Effectiveness as a relation of Number of Fins for  $t^* = 0.0333$  Orientation B.

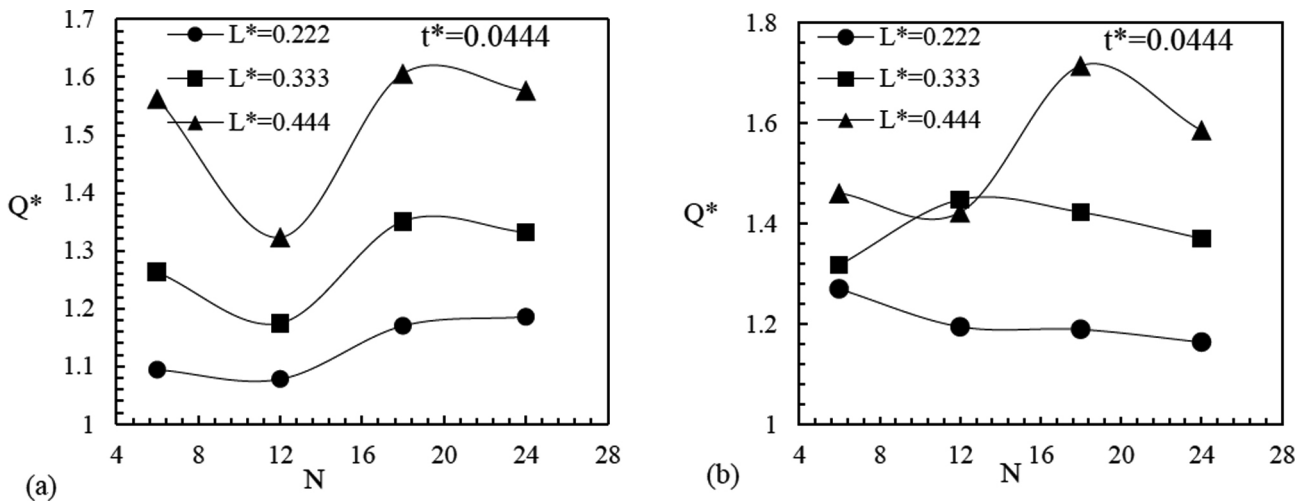


Figure 17. a) Effectiveness as a relation of Number of Fins for  $t^* = 0.0444$ , Orientation A; b) Effectiveness as a relation of Number of Fins for  $t^* = 0.0444$  Orientation B.

SS is given for  $N = 6$  &  $12$  for orientation-B, it is observed that there is 1.5–8.8% loss when Stainless steel was simulated for the same model, the decrease of effectiveness for a model is in direct proportionality to its fin length.

Figure 15-17 represents the effectiveness versus number of fins plot for changing fin length and fin thickness for both the orientations. Figure 15 a) is showing the plots of effectiveness with respect to number of fins (inverse of fin spacing) for orientation-A for  $t^* = 0.0222$ , from the plot it can be inferred that a maximum value of effectiveness exists in

the chosen domain of the current research. Orientation-A is showing a drop till  $N = 12$  and the gradual increase in the effectiveness, the optimum effectiveness for  $L^* = 0.444$  is 1.61 for  $N = 6$ , for  $L^* = 0.333$  &  $0.222$  the optimum value of effectiveness is achieved at  $N = 24$  i.e.  $Q^* = 1.59$  &  $1.18$  respectively. From Figure 15(b), this is plot of effectiveness with respect to number of fins for  $t^* = 0.0222$  with orientation-B, it can be concurred that the two plots are rather different, it can be explained by the behaviour of thermal boundary layer and fluid flow which is different for geometrically different arrangement of fins. For orientation-B, the maximum effectiveness is achieved at  $N = 12$  for  $L^* = 0.444$  and  $0.333$  with the values  $Q^* = 1.86$  &  $1.33$  respectively. The effectiveness for the  $L^* = 0.222$  is increasing in linear fashion with low slope increasing till the value of  $Q^* = 1.13$ .

Figure 16(a) is representing the effectiveness of orientation-A for  $t^* = 0.0333$ , it is observed that for all the fin length, the maximum effectiveness is achieved for maximum number of fins  $N = 24$ . Figure 16(b) is representing the effectiveness of orientation-B for  $t^* = 0.0333$ , in this orientation the optimum value of effectiveness is achieved at  $N = 18$  for  $L^* = 0.333$  &  $0.444$  with values being  $Q^* = 1.42$  &  $1.79$  respectively, adding to the exception for  $L^* = 0.222$  the maximum value is at  $N = 12$  with  $Q^* = 1.26$ . Figure 17(a) and Figure 17(b) shows the effectiveness plot with respect to number of fins for orientation-A and B respectively. From Figure 17(a) it can be observed that for  $L^* = 0.444$  &  $0.333$  the maximum value is for  $N = 18$  and for  $L^* = 0.222$ , the optimum value of effectiveness is more or less same for  $N = 18$  and  $24$ . From Figure 17(b) the maximum effectiveness for  $L^* = 0.444$  is  $Q^* = 1.72$  at  $N = 18$ , for  $L^* = 0.333$  is  $Q^* = 1.45$  at  $N = 12$  and for  $L^* = 0.222$  is  $Q^* = 1.28$  at  $N = 6$ . By looking at the effectiveness plots, after careful observation, it can be deduced that for particular fin thickness as the fin length is decreasing the value optimum number of fins is decreasing as well. This implies that for special constraints

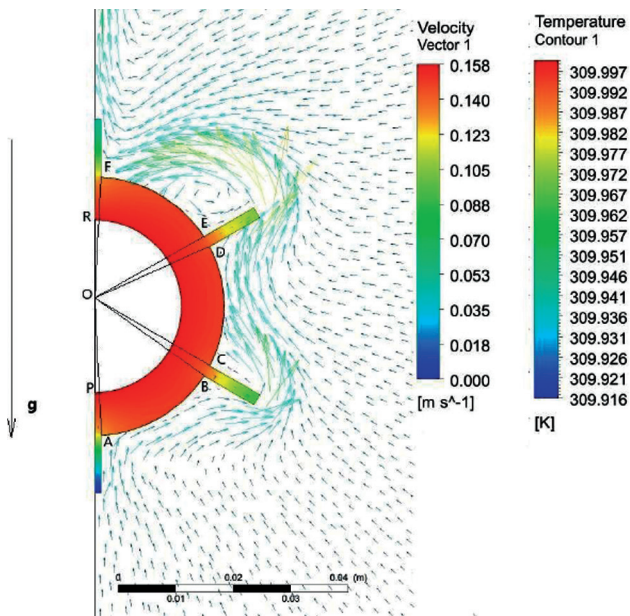


Figure 18. Temperature contour of cross-section for Fin-tube system with Velocity vectors for  $N = 6$ ,  $L^* = 0.222$  &  $t^* = 0.0444$ .

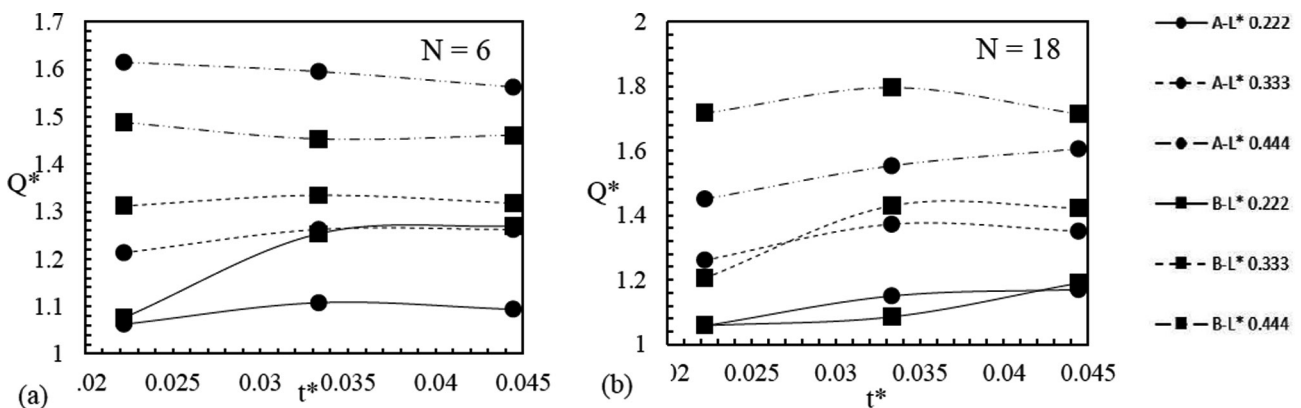
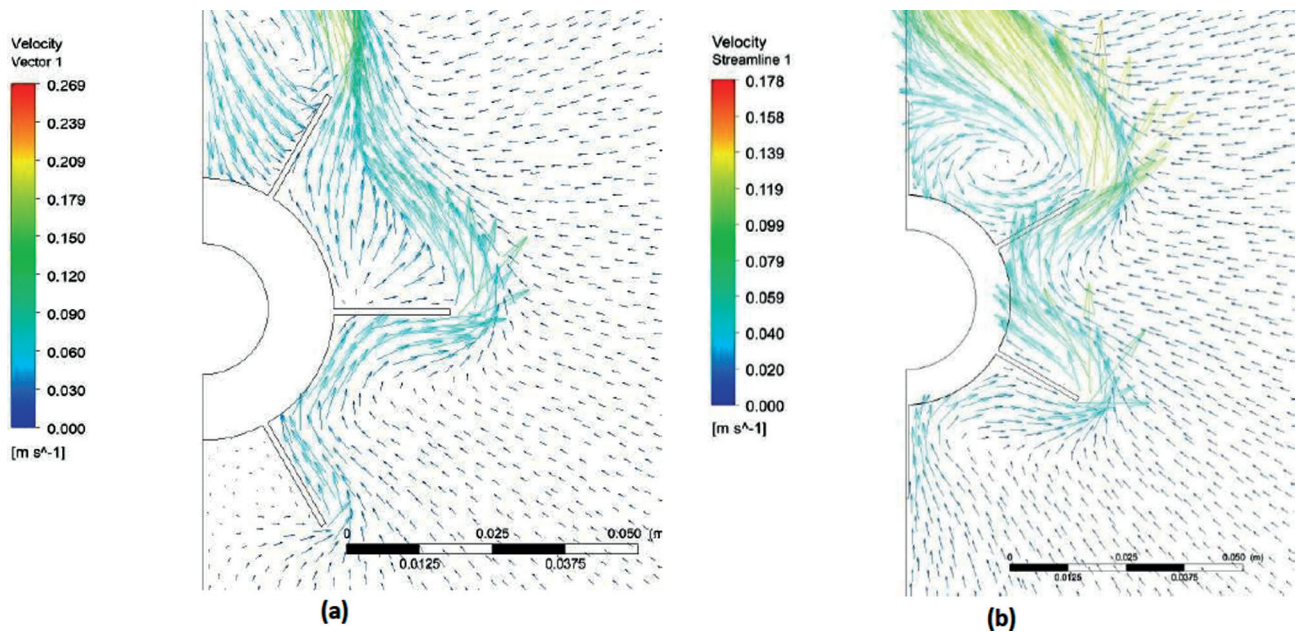
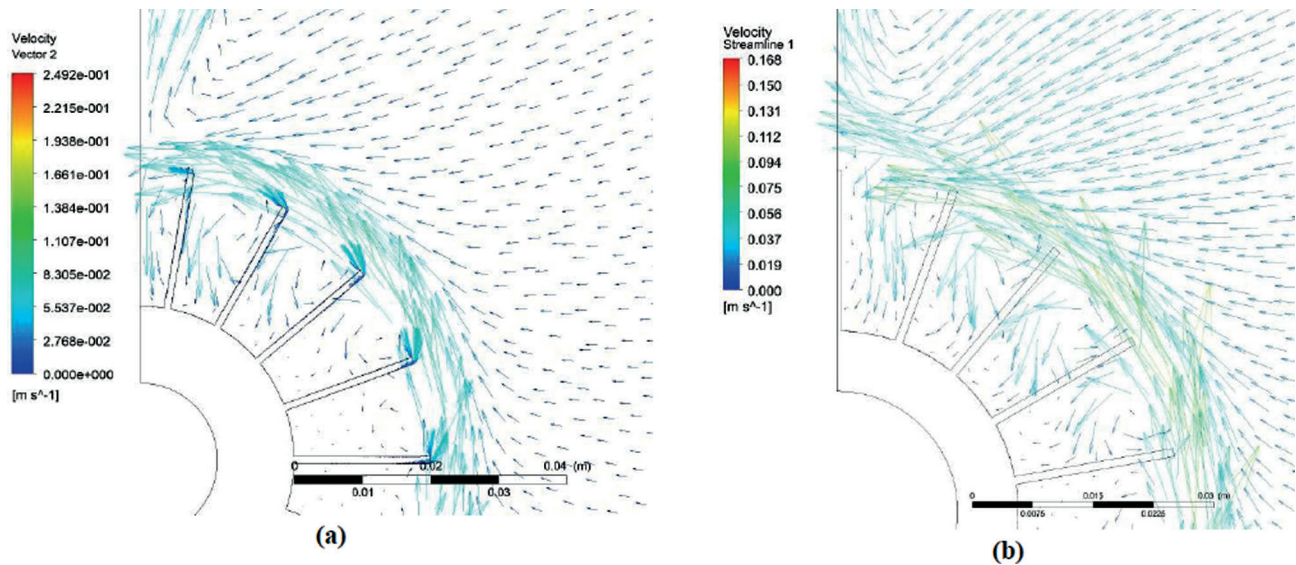


Figure 19. a) Effectiveness shown with respect to non-dimensional fin length comparing Orientation A&B for  $N = 6$ ; b) Effectiveness shown with respect non-dimensional fin length comparing Orientation A&B for  $N = 18$ .



**Figure 20.** a) Velocity Vectors for  $N = 6$ ,  $L^* = 0.444$  and  $t^* = 0.0222$ , Orientation A; b) Velocity Vectors for  $N = 6$ ,  $L^* = 0.444$  and  $t^* = 0.0222$ , Orientation B.



**Figure 21.** a) Velocity Vectors for  $N = 18$ ,  $L^* = 0.444$  and  $t^* = 0.0222$  Orientation A; b) Velocity Vectors for  $N = 18$ ,  $L^* = 0.444$  and  $t^* = 0.0222$  Orientation B.

where the overall diameter of the system is limited, applying more of fins to the outer surface will increase the overall heat transfer rate but up to a certain extend.

Figure 18 is showing the temperature contour in the solid cross-section of the fin-tube system and velocity vectors showing the change direction given by arrow heads and length of the arrow tail is corresponding to the magnitude of velocity. By the authors' knowledge, the system

having longitudinal fins on the outer surface of the horizontal hollow cylinder with inner wall at isothermal condition have not been investigated thoroughly, it can be explained because the gravitational component is perpendicular to the axis of the cylinder which makes the flow of air particles complex which is non-existing in the thermal systems with annular fins at the outer surface. Therefore, the thermal characteristics of the system are not forming

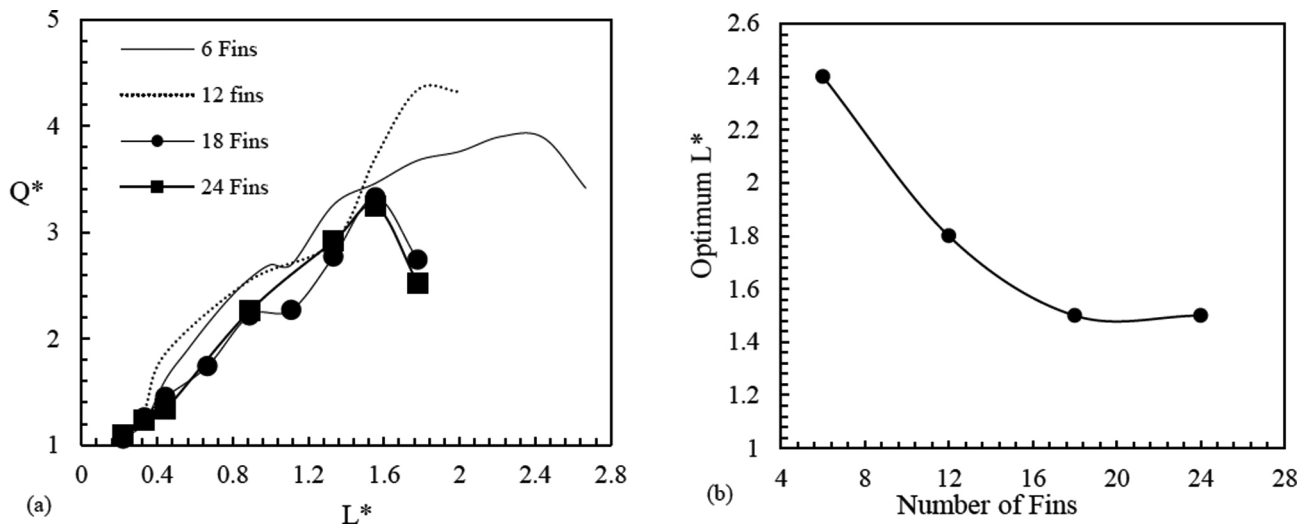


**Figure 22.** a) Effectiveness versus Non-dimensional fin length for  $N = 6$  to  $24$  for  $t^* = 0.0222$ ; b) Optimum fin length as a function of number of fins.

**Table 5.** The value of the optimum fin lengths

N (number of fins)	$L^*_{opt}$	$Q^*_{opt}$
6	2.4	3.88
12	1.8	4.34
18	1.5	3.32
24	1.5	3.24

a set pattern. This insufficiency of getting a set sequence is absent for annular fins on the outer surface of the hollow horizontal cylinder [27], the solution of those cases is also possible using analytical relations [26]. This complexity can be assessed by the behaviour of the velocity vectors shown in Figure 18. Moving from point A to B the fluid is normal flowing upwards, but between point B and C, the angular distance having the longitudinal fins is resisting the smooth flow hence, the temperature of the external surface of the system is not changing the same way it is changing from A to B or from C to D.

Figure 19 is showing a direct contrast between the orientation-A & B, with plots of effectiveness versus the non-dimensional fin thickness for  $N = 6$  and  $N = 18$ , however, from the plots it is still complex to generalize the whole notion. On Comparison, for  $N = 6$ , orientation-A came out to be more effective than orientation-B for long fins, For  $N = 18$ , orientation-B was more effective that orientation-A for long fins. The maximum effectiveness was  $Q^* = 1.62$  for  $L^* = 0.444$  and  $t^* = 0.0222$  for 6 fins and for 18 fins the optimum effectiveness was  $Q^* = 1.79$  for  $L^* = 0.444$  and  $t^* = 0.0333$ .

Figure 20 shows the velocity vector comparison for the two orientations, from the contours it is deduced that for  $L^* = 0.444$  and  $t^* = 0.0222$ , the velocity attained by the air particles is higher for orientation-A. From Figure 21 it can be inferred that for  $L^* = 0.444$  and  $t^* = 0.0222$ , at the end of the tip of fins the air particles are forming small vortices which enhances the rate of heat transfer by creating microturbulences.

Further, in the research it was deduced that the fin thickness for the case of natural convection in the geometry of longitudinal fins at the outer surface of the hollow cylinder is not a factor of importance, because it is only changing the conductive thermal resistance of the overall fin-tube system which is not an appreciable contributor to the overall thermal resistance. Therefore, fin length becomes the factor on which the rate of heat transfer is depending on with respect to a particular number of fins. Figure 22 a) represents the fin optimization plot. From the figure, it can be seen that the plot is effectiveness versus non-dimensional fin length for varying number of fins. Since, the fin thickness is not the key factor for this investigation a moderate fin thickness  $t^* = 0.0222$  was selected for geometries. Figure 22 b) is showing the variation of optimum fin length with respect to the number of fins, as it is easily noticeable that the optimum fin length is decreasing with the number of fins.

## CONCLUSION

In the present investigation, thermal characteristics like heat flux, effectiveness, thermal boundary layer, small vortices formation and velocity streamlines have been

represented and thoroughly discussed after numerically solving Natural convection on a fin-tube system having longitudinal fin on the outer surface of a horizontal hollow cylinder while the fin geometry was varying for constant Rayleigh number  $1.77 \times 10^5$ , i.e. in laminar range, using CFD software Ansys Fluent. Simulations were performed by varying fin length to outer diameter ratio ( $L^*$ ) from 0.222 to 2, fin thickness to outer diameter ( $t^*$ ) was varied from 0.022 to 0.044 and the number of fins was varied from  $N = 6$  to  $N = 24$ .

The results of this particular research can be used as a benchmark for thermal system designers in the future, the study insights many facts involving the design of systems having natural convection which can be used in the field of computer processor cooling, microprocessor cooling and also phase change material heat exchangers. This study can be concluded by stating that the behavior of airflow for natural convection around longitudinal fins is complex in comparison to annular fins.

- Heat Flux is decreasing with an increase in the number of fins for both orientations and heat flux is maximum for 6 fins.
- Optimization is possible for effectiveness by constraining either the number of fins or the fin length.
- For a fixed fin length there exist an optimum fin thickness and an optimum number of fins.
- The Maximum effectiveness in the range of fin length to outer diameter ratio ( $L_f/D_o$ ) of 0.22 to 0.44 was found to be 1.86 and that was for orientation-B at 12 fins.
- The Maximum decrease in effectiveness for using stainless steel instead of aluminium is 8.83%.
- The optimum fin length decreases as the number of fins increase and is getting constant as the number of fins is reaching 30.
- For a fixed number of fins there exist an optimum fin length and maximum effectiveness, the maximum possible effectiveness for the taken fin-tube system is 4.34 for 12 fins.

## NOMENCLATURE

Outer diameter of the tube, m  
 Inner diameter of the tube, m  
 Fin spacing, m  
 Ratio of total diameter of the fin-tube system and outer diameter of tube  
 Length of fin, m  
 Thickness of fin, m  
 Number of fins  
 Temperature of inner wall, °C  
 Temperature of the free stream, °C  
 Temperature of outer surface, °C  
 Bulk Temperature of the fluid, °C  
 Diameter of the domain, m

Axial length of the system, m  
 Non-dimensional fin thickness,  $t^* = t/D_o$   
 Non-dimensional fin length,  $L^* = L_f/D_o$   
 Heat transfer per unit area, simulations result,  $W/m^2$   
 Heat transfer per unit area of tube of same diameter without fins, simulation result,  $W/m^2$   
 Total rate of heat transfer, W  
 Total rate of heat transfer of tube of same diameter without fins, W  
 Non-dimensional heat flux,  $q^* = q/q_o$   
 Effectiveness (or non-dimensional heat transfer),  $Q^* = Q/Q_o$   
 Thermal conductivity of Aluminium,  $W/m.K$   
 Thermal conductivity of Stainless steel,  $W/m.K$   
 Velocity in i direction, m/s  
 Directional components in i direction, m  
 Density of air,  $Kg/m^3$   
 Density of air at free stream,  $Kg/m^3$   
 Gravitational acceleration component in i direction,  $m/s^2$   
 Specific heat of air,  $J/kg.K$   
 Gas constant for atmospheric air,  $J/kg.K$   
 Velocity components in x, y and z direction respectively, m/s  
 Atmospheric pressure, Pa  
 Thermal conductivity of solid,  $W/m.K$   
 Thermal conductivity of fluid,  $W/m.K$   
 Temperature of solid at the interface, °C  
 Temperature of fluid at the interface, °C  
 Convective heat transfer coefficient,  $W/m^2.K$   
 Total surface area,  $m^2$   
 Surface area of fin,  $m^2$   
 Surface area of unfinned region,  $m^2$   
 Nusselt number  
 Nusselt number based on outer diameter  
 Rayleigh number based on outer diameter,  

$$Ra_D = \frac{g\beta\Delta T D^3}{\alpha\nu}$$
 Thermal expansivity of air,  $1/K$   
 Temperature difference,  $\Delta T = T_w - T_\infty$ , °C  
 Thermal diffusivity of air,  $m^2/s$   
 Prandtl number of air  
 Rayleigh number based on fin spacing,  

$$Ra_s = \frac{g\beta(T_w - T_\infty) S^3}{\alpha\nu} \left(\frac{S}{D}\right)$$
 Kinematic viscosity of air,  $m^2/s$

## AUTHORSHIP CONTRIBUTIONS

Authors equally contributed to this work.

## DATA AVAILABILITY STATEMENT

The authors confirm that the data that supports the findings of this study are available within the article. Raw

data that support the finding of this study are available from the corresponding author, upon reasonable request.

## CONFLICT OF INTEREST

The author declared no potential conflicts of interest with respect to the research, authorship, and/or publication of this article.

## ETHICS

There are no ethical issues with the publication of this manuscript.

## REFERENCES

- [1] Goldstein RJ, Ibele WE, Patankar SV, Simon TW, Kuehn TH, Stryowski PJ, et al. Heat transfer – A review of 2005 literature. *Int J Heat Mass Tranf* 2010;53:4397–4447. [\[CrossRef\]](#)
- [2] Ali HM, Ashraf MJ, Giovanelli A, Irfan M, Bin Irshad T, Hamid HM, et al. Thermal management of electronics: An experimental analysis of triangular, rectangular and circular pin-fin heat sinks for various PCMs. *Int J Heat Mass Tranf* 2018;123:272–284. [\[CrossRef\]](#)
- [3] Bhowmik H, Tou KW. Experimental study of transient natural convection heat transfer from simulated electronic chips. *Exp Therm Fluid Sci* 2005;29:485–492. [\[CrossRef\]](#)
- [4] Bondareva NS, Buonomo B, Manca O, Sheremet MA. Heat transfer inside cooling system based on phase change material with alumina nanoparticles. *Appl Therm Eng* 2018;144:972–981. [\[CrossRef\]](#)
- [5] Bondareva NS, Sheremet MA. Conjugate Heat Transfer in the PCM-based heat storage system with finned copper profile: Application in electronics cooling. *Int J Heat Mass Tranf* 2018;124:1275–1284. [\[CrossRef\]](#)
- [6] Kasza K, Malinowski L, Krolikowski I. Optimization of pin fin heat sink by application of CFD simulations and DOE methodology with neural network approximation. *Int J App Mech Eng* 2013;18:365–381. [\[CrossRef\]](#)
- [7] Kraus AD, Aziz A, Welty J. *Extended Surface Heat Transfer*. New York: John Wiley & Sons, 2001. [\[CrossRef\]](#)
- [8] Churchill SW, Chu HS. Correlating equations for laminar and turbulent free convection from a horizontal cylinder. *Int J Heat Mass Transf* 1975;18:1049–1053. [\[CrossRef\]](#)
- [9] Morgan VT. Heat transfer by natural convection from a horizontal isothermal circular cylinder in air. *Heat Transf Eng* 1997;18:25–33. [\[CrossRef\]](#)
- [10] Kwon SS, Kuehn TH. Conjugate natural convection heat transfer from a horizontal cylinder with a long vertical longitudinal fin. *Numer Heat Transf* 1983;6:85–102. [\[CrossRef\]](#)
- [11] Tolpadi K, Kuehn TH. Computation of conjugate three-dimensional natural convection heat transfer from a transversely finned horizontal cylinder. *Numer Heat Transf Part A Appl* 1989;16:1–13. [\[CrossRef\]](#)
- [12] Yuncu H, Anbar G. An experimental investigation on performance of rectangular fins on a horizontal bas in free convection heat transfer. *Heat Mass Tranf* 1998;33:507–514. [\[CrossRef\]](#)
- [13] Abu-Hijleh AK. Natural convection and entropy generation from a cylinder with high conductivity fins. *Numer Heat Transf Part A-Appl* 2001;39:405–432. [\[CrossRef\]](#)
- [14] Abu-Hijleh AK. Optimization of natural convection heat transfer from a cylinder with high conductivity fins. *Numer Heat Transf Part A-Appl* 2003;43:65–82. [\[CrossRef\]](#)
- [15] Wu JM, Tao WQ. Numerical computation of laminar natural convection heat transfer around a horizontal compound tube with external longitudinal fins. *Heat Transf Eng* 2007;28:93–102. [\[CrossRef\]](#)
- [16] Senapati JR, Dash SK, Roy S. Numerical investigation of natural convection heat transfer over annular finned horizontal cylinder. *Int J Heat Mass Transf* 2016;96:330–345. [\[CrossRef\]](#)
- [17] Acharya S, Agrawal S, Dash SK. Numerical analysis of natural convection heat transfer from a vertical hollow cylinder suspended in air. *J Heat Transf* 2018;140:052501. [\[CrossRef\]](#)
- [18] Foroushani S, Naylor D, Wright JL. Heat transfer correlations for laminar free convection in vertical channels with asymmetrically heated isothermal walls. *Heat Tranf Eng* 2018;41:418–432. [\[CrossRef\]](#)
- [19] Yildiz S. Investigation of natural convection heat transfer at constant heat flux along a vertical and inclined plate. *J Therm Eng* 2018;4:2432–2444. [\[CrossRef\]](#)
- [20] Rath S, Dash SK. Laminar and turbulent natural convection from a stack of thin hollow horizontal cylinders: A numerical study. *Num Heat Tranf Part A: Appl* 2019;75:753–775. [\[CrossRef\]](#)
- [21] Menni Y, Chamkha AJ, Azzi A. Nanofluid transport in porous media: A review. *Spec Top Rev Porous Media* 2018;9:1–16. [\[CrossRef\]](#)
- [22] Gorla RSR, Chamkha A. Natural convection boundary layer flow over a nonisothermal vertical plate embedded in a porous medium saturated with a nanofluid. *Nanoscale Microscale Thermophys Eng* 2011;15:81–94. [\[CrossRef\]](#)
- [23] Mahfoud B, Bendjaghloli A. Natural convection of a nanofluid in conical container. *J Therm Eng* 2018;4:1713–1723. [\[CrossRef\]](#)
- [24] Zaraki A, Ghalambaz M, Chamka AJ, Ghalambaz M, De Rossi D. Theoretical analysis of natural

- convection boundary layer heat and mass transfer of nanofluids: Effects of size, shape and type of nanoparticles, type of base fluid and working temperature. *Adv Powder Technol* 2015;26:935–946. [\[CrossRef\]](#)
- [25] Dogonchi AS, Tayebi T, Chamkha AJ, Ganji DD. Natural convection analysis in a square enclosure with a wavy circular heater under magnetic field and nanoparticles. *J Therm Anal Calorim* 2020;139:661–671. [\[CrossRef\]](#)
- [26] Tsubouchi T, Masuda H. Natural Convection Heat transfer from horizontal cylinders with circular fins. 1970 Proc. 6<sup>th</sup> Int Heat Transf Conf Paper NC 1.10. [\[CrossRef\]](#)
- [27] Krishnayatra G, Tokas S, Kumar R, Zunaid M. 3 Dimensional CFD analysis of Laminar Flow Natural Convection of Hollow Cylinder with Annular Fins. Proc. 5<sup>th</sup> World Cong Mech Chem Mat Eng HTFF-181 2019, 1–10. [\[CrossRef\]](#)
- [28] Lin S, Shih T, Chang RR, Chen Z. Optimization of cooling effects with fins of variable cross sections. *Num Heat Tranf Part A: App* 2016;69:850–858. [\[CrossRef\]](#)
- [29] Ali M, Nuhait A, Almuzaiqer R. The effect of square tube location in a vertical array of square tubes on natural convection heat transfer. *Heat Tranf Eng* 2017;39:1036–1051. [\[CrossRef\]](#)
- [30] Davies III WA, Hrnjak P. Heat transfer in a large, inclined, flattened-tube steam condenser. *Heat Tranf Eng* 2019;1443–1456. [\[CrossRef\]](#)
- [31] Krishne Gowda GBM, Rajagopal MS, Aswatha, Seethramu KN. Numerical studies on natural convection in a trapezoidal enclosure with discrete heating. *Heat Tranf Eng* 2019;595–606. [\[CrossRef\]](#)
- [32] Rath S, Dash SK. Laminar and turbulent natural convection from a stack of thin hollow horizontal cylinders: A numerical study. *Num Heat Tranf Part A: App* 2019;75:753–775. [\[CrossRef\]](#)
- [33] Yildiz S., Yuncu H. An experimental investigation on performance of annular fins on a horizontal cylinder in free convection heat transfer. *Heat Mass Tranf* 2004;40:239–251. [\[CrossRef\]](#)
- [34] S. C. laminar free convection around a horizontal cylinder with external longitudinal fins. *Heat Tranf Eng* 2004;25:45–53. [\[CrossRef\]](#)
- [35] Shah RK, Sekulic DP. *Fundamentals of Heat Exchanger Design*. New York: John Wiley & Sons, 2003. [\[CrossRef\]](#)
- [36] Incropera FP, Dewitt DP, Bergman TL, Levine AS. *Fundamentals of Heat and Mass Transfer*. 6<sup>th</sup> ed. New York: John Wiley & Sons, 2007.
- [37] Menni Y, Azzi A., Zidani C. Computational analysis of heat transfer and fluid flow characteristics over flat bars of different heights. *Revue des Energies Renouvelables* 2016;19:34–366.
- [38] Menni Y, Chamkha AJ, Lorenzini G, Benyoucef M. Computational fluid dynamics based numerical simulation of thermal and thermo-hydraulic performance of a solar air heater channel having various ribs on absorber plates. *Math Model Eng Problems* 2019;6:170–174. [\[CrossRef\]](#)
- [39] Menni Y, Azzi A. Computational fluid dynamical analysis of turbulent heat transfer in a channel fitted with staggered V-Shaped baffles. *World J Model Sim* 2018;14:108–123.
- [40] Menni Y, Azzi A, Chamkha AJ, Harmand S. Analysis of Fluid Dynamics and Heat Transfer in a Rectangular Duct with Staggered Baffles. *J Appl Comp Mechanics* 2019;5:231–248.
- [41] Zunaid M, Jindal A, Gakhar D, Sinha A. Numerical Study of Pressure Drop and Heat Transfer in a straight rectangular and semi cylindrical projections micro-channel heat sink. *J Therm Eng* 2017;3:1453–1465. [\[CrossRef\]](#)
- [42] Acharya S, Dash SK. Natural convection heat transfer from a short or long, solid or hollow horizontal cylinder suspended in air or placed on ground. *J Heat Transf* 2017;139:072501. [\[CrossRef\]](#)
- [43] Morgan V. T. *The Overall Convective Heat Transfer from Smooth Circular Cylinders*. New York: Academic Press, 1975;11:199–264. [\[CrossRef\]](#)
- [44] Sahel D, Ameer H, Kamla Y. A numerical study of fluid flow and heat transfer over a fin and flat tube heat exchangers with complex vortex generators. *Eur Phys J Appl Phys* 2017;78:34805. [\[CrossRef\]](#)
- [45] Boukhadia K, Ameer H, Sahel D, Bozit M. Effect of the perforation design on the fluid flow and heat transfer characteristics of a plate fin heat exchanger. *Int J Therm Sci* 2018;126:172–180. [\[CrossRef\]](#)
- [46] Alem K, Sahel D, Nemdili A, Ameer H. CFD investigations of thermal and dynamic behaviours in a tubular heat exchanger with butterfly baffles. *Fron Heat Mass Tranf* 2018;10:27. [\[CrossRef\]](#)
- [47] Ameer H, Menni Y. Laminar cooling of shear thinning fluids in horizontal and baffled tubes: Effect of perforation in baffles. *Therm Sci Eng Prog* 2019;14:100430. [\[CrossRef\]](#)
- [48] Ameer H. Effect of the baffle inclination on the flow and thermal fields in channel heat exchangers. *Results Eng* 2019;3:100021. [\[CrossRef\]](#)